Int. J. Electrochem. Sci., 14 **(2019)** 427 – 440, doi: 10.20964/2019.01.11

International Journal of
ELECTROCHEMICAL
SCIENCE
www.electrochemsci.org

Investigations of Micro-Dimples Prepared by the Multiple Sandwich-Like Electrochemical Micromachining

Xifang Zhang[1,*], *Hua Li*[1,2], *Zhen Yin*[1], *Ren Kun*[1]

[1] College of Mechanical Engineering, Suzhou University of Science and Technology, Suzhou 215009, PR China
[2] Suzhou Key Laboratory of Precision and Efficient Manufacturing Technology, Suzhou 215009, PR China
[*]E-mail: zhxflove@126.com

Received: 23 September 2018 / *Accepted:* 18 October 2018 / *Published:* 30 November 2018

Micro-dimples are widely used in tribology as a surface texture and play a significant role in improving interfacial performance, allowing for reducing friction and wear, reducing vibration and noise of various mechanical components. Through-mask electrochemical micromachining (TMEMM) is a feasible method for preparing micro-dimples. However, in TMEMM, the island phenomenon and poor dimensional uniformity often occur in micro-dimples, which will weaken tribological properties. Sandwich-like electrochemical micromachining (SLEMM) could be used to fabricate micro-dimples, but these tend to be shallow and the maximum depth of 4 μm for micro-dimples could be machined with the increase of machining time and applied voltage, because of the electrolytic products accumulated on the enclosed unit. In this investigation, multiple machining process of SLEMM is employed to remove the electrolytic products and generate deep micro-dimples. The experimental results showed that deep micro-dimples could be fabricated with multiple cycles of SLEMM, and at 15 V applied voltage and the 12th cycles process of SLEMM, the depth and diameter of micro-dimples are 18 μm and 120 μm, respectively. In addition, numerical simulations and experimental results verified that the island phenomenon can be avoided and dimensional uniformity of micro-dimples could be enhanced by using SLEMM, compared with TMEMM.

Keywords: Micro-dimples, Through-mask electrochemical micromachining (TMEMM), Multiple, Island, Dimensional uniformity, Sandwich-like electrochemical micromachining (SLEMM)

1. INTRODUCTION

Recent innovations in the area of micro fabrication have created a unique opportunity for manufacturing structures. Nowadays, surface texturing at the micro range of micro-dimples, micro-grooves, micro-pillars and micro-prisms has represented an advanced technology in many engineering fields. The modern micro-machining technology makes it possible to optimize the interface performance by precisely controlling the shape and dimensions of surface texture [1]. Currently, surface texture has been involved in reducing friction, anti-wear, increasing friction, reducing vibration, anti-creeping [2-4].

As one type of surface texture, micro-dimples have been extensively used in various industries for enhancement in the performance and usability of mechanical systems, such as improving biological, optical, tribological as well as thermal properties. A substantial number of techniques exist for micro-dimple pattern fabrication, such as milling [5], conventional micro-turning [6], chemical etching [7], laser beam machining [8], electric discharge machining [9], and electrochemical micromachining (EMM) [10]. Compared with other methods, EMM is a promising technique, with advantages such as high machining efficiency, independence of material hardness and toughness, the absence of a heat-affected layer, a lack of residual stresses, cracks, tool wear and burrs, and low production cost.

Through-mask electrochemical micromachining (TMEMM) is also a popular method for preparing micro-dimples. Using this method, Madore and Landolt [11] fabricated arrays of hemispherical cavities on titanium. Hao et al. [12] generated micro-dimples on cylindrical surfaces at a feature size of 40 μm. Nouraeiz and Roy [13] used a patterned metallic cathode to apply micro features to unmasked substrates, in which the workpiece is placed in an electrochemical reactor in close proximity to the cathode. Costa and coauthors [14] proposed a maskless electrochemical texturing method to simultaneously prepare a large number of micro-dimples, which can be regarded as an adaptation of jet ECM to texture surfaces by using a masked tool. Zhu [15] proposed a method in which a mask with a patterned insulation plate, coated with metal film as cathode, is closely attached to the workpiece plate instead of bonding a photoresist layer on to the workpiece, as is done in the conventional TMEMM. Qu [16] prepared micro-dimple arrays by TMEMM with a flexible PDMS mask, which might be reused.

It has been found that a surface processing micro-dimples with optical geometry, density, and area ratio is more effective for enhancing tribological performance. Therefore, the machining accuracy of surface texturing is a key factor for a high-quality textured surface [17]. However, in TMEMM, the island formation and non-uniform dimensional distribution of micro-dimples are inevitable. Shenoy [18] investigated the island formation during TMEMM and observed that the island was most likely to occur with a low aspect ratio and low mask thickness. Wang [19] also reported the similar phenomenon and indicated that the island of micro-dimples can be dissolved by prolonging the machining time. However, the micro-dimple depth and diameter will be simultaneously increased with the prolonging machining time, which will reduce machining accuracy of micro-dimples and affect tribological performance. Chen [20] developed an auxiliary electrode with a positive potential to enhance the uniformity of distribution of the electrical field on the workpiece during TMEMM.

The sandwich-like electrochemical micromachining (SLEMM) can be used to fabricate micro-dimples. However, the micro-dimples obtained during SLEMM tend to be shallow, and the maximum depth of 4 μm for micro-dimples could be prepared with the increase of applied voltage and machining time, because of the nonconductive insoluble electrolytic products and gas bubbles accumulated on the workpiece surface during the enclosed unit of SLEMM [21]. Though the shallow micro-dimples can raise and reduce the coefficient of friction between mating components [22], the deep micro-dimples are needed to be machined for tribological applications [23].

In this investigation, the multiple cycles machining process of SLEMM is employed to remove electrolytic products and generate deep micro-dimples. Moreover, numerical simulations and experiments have been performed to explore the profiles and dimensional uniformity of micro-dimples fabricated using TMEMM and SLEMM. The schematic view of the proposed multiple SLEMM is illustrated in Fig. 1 as follows:

(1) The dry-film mask with patterned through-holes is firmly laminated to the anode workpiece surface (Fig. 1a).

(2) The cathodic tool keeps in close contact with the dry-film mask, and the dissolution of the anode workpiece surface takes place in the enclosed unit of SLEMM with an appropriate combination of machining parameters (Fig. 1b).

(3) The cathodic tool moves up to remove the gas bubbles and nonconductive insoluble electrolytic products, and to renew the electrolyte in the gap (Fig. 1c).

(4) The cathodic tool moves down until it is in close contact with the dry-film mask, and the machining process of SLEMM is done (Fig. 1d).

(5) The multiple cycles of SLEMM (Fig. 1c, d) are repeated until the desired micro-dimples are achieved (Fig. 1e).

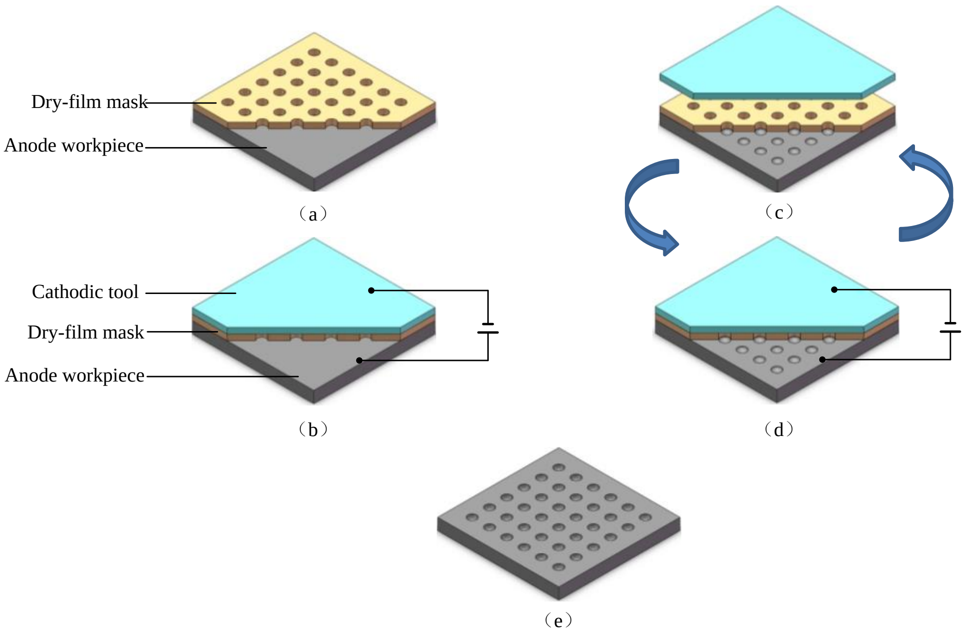

Figure 1. The schematic view of the multiple SLEMM

2. EXPERIMENTAL

2.1 Modeling

The simplified schematic models of SLEMM and TMEMM are shown in Fig. 2 and Fig. 3 respectively. In the numerical simulation, the reaction rate distribution is assumed to be determined by an electric potential. The following conditions and assumptions are made [18]:

(1) The electrolyte conductivity, κ, keeps constant.

(2) The concentration gradient in the bulk electrolyte is negligible.
(3) The current efficiency of metal dissolution keeps constant.
(4) The thermal effects could be ignored during the EMM process.

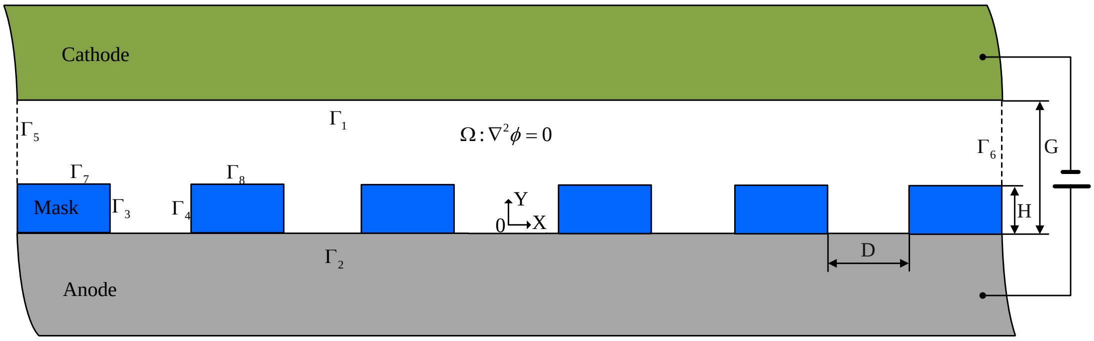

Figure 2. Schematic view of TMEMM

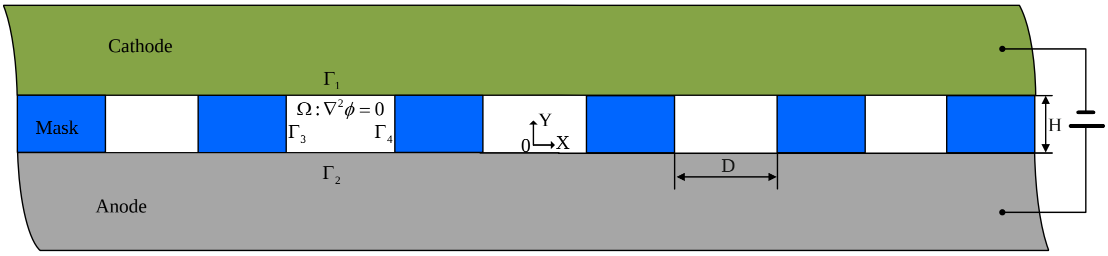

Figure 3. Schematic model of SLEMM

Based on electric field theory, the electric potential ϕ in the inter-electrode gap is governed by Laplace's equation:

$$\Omega : \nabla^2 \phi = \frac{\partial^2 \phi}{\partial x^2} + \frac{\partial^2 \phi}{\partial y^2} = 0 \quad (1)$$

Table 1. Boundary conditions for SLEMM and TMEMM

SLEMM		TMEMM	
$\phi\vert\Gamma_2 = V_a$	(2)	$\phi\vert\Gamma_2 = V_a$	(5)
$\phi\vert\Gamma_1 = 0$	(3)	$\phi\vert\Gamma_1 = 0$	(6)
$\frac{\partial \phi}{\partial n}\vert\Gamma_{3,4} = 0$	(4)	$\frac{\partial \phi}{\partial n}\vert\Gamma_{3,4,7,8} = 0$	(7)
		$\frac{\partial \phi}{\partial n}\vert\Gamma_{5,6} \approx 0$	(8)

The boundary conditions for SLEMM and TMEMM are listed in Table 1, where V_a is the voltage between the anode and the cathode (the kinetic resistance at the electrodes is neglected) and n is the unit normal vector to the surface.

The current density i is given by Ohm's law:

$$i = \kappa E = -\kappa \Delta \varphi \quad (9)$$

where κ is the electrolyte conductivity, E is the electric field intensity, φ is the potential in machining area.

The material removal rate v is determined by Faraday's law:

$$\upsilon = \eta\omega i \qquad (10)$$

where ω is the volume electrochemical equivalent of the anodic metal, and η is the current efficiency of metal dissolution, which is assumed to be constant at 100%.

2.2 Numerical simulation

The anode workpiece is divided into several independent small processing zones by the insulated mask with through-holes. Therefore, each small processing zone can be regarded as an independent micro-electrolytic cell in EMM. The finite element method is employed to solve the boundary conditions, and the COMSOL Multiphysics is used as the numerical technique. To investigate the electrical field intensity distribution for SLEMM and TMEMM, the model was analyzed under the conditions shown in Table 2.

Table 2. The Simulated parameters with SLEMM and TMEMM

Fixed parameter	Value
Voltage between electrodes, V_a	6 V
Electrolyte conductivity, κ	8.7 S/m
Volume electrochemical equivalent of anode, ω	0.0348 $mm^3/(A\cdot s)$
Diameter of through-holes in dry-film mask, D	100 μm
Thickness of dry-film mask, H	50 μm
Inter-electrode gap, G (TMEMM)	2 mm
Boundary update time, Δt	0.1 s

Fig. 4 shows the normalized electrical field intensity distribution within a single through-hole on the initial anodic workpiece surface for SLEMM and TMEMM. The normalized electrical field intensity within a single through-hole of the mask is defined as E/E_{max}, where E is the electrical field intensity of every key point in the single through-hole on the workpiece surface, and E_{max} is the maximum electric field intensity. It can be found that the electrical field intensity distribution is non-uniform within a single through-hole on the workpiece surface during TMEMM and that the electrical field intensity at the mask edge is larger than that at the feature center, in which the electrical field intensity at the center is 0.8 times higher than that at the mask edge. Thus, the initial current density distribution at the mask edge is higher than that at the center in a single thorough-hole on the workpiece surface, and the material removal rate at the mask edge is faster than that at the center. These imply that the "island" will be formed in the center of the micro-dimple. However, a mutational electrical field intensity distribution occurs in a single through-hole at the mask edge in SLEMM, and the electrical field intensity distribution is uniform in a single through-hole on the initial workpiece surface. Which leads to the even current density distribution in a single through-hole on the mask, the material removal rate is uniform within a single through-hole on the mask, and the bottom of the micro-dimple is flat. Therefore, compared with TMEMM, the

SLEMM could effectively eliminate the "island" phenomenon theoretically.

The normalized electrical field intensity E_i/E_{imax} is introduced to analyze the electrical field intensity distribution on the whole workpiece surface, where E_i is the electrical field intensity at the center of each through-hole on the whole workpiece surface, and E_{imax} represents the maximum electrical field intensity at the center of all through-holes on the whole workpiece surface. The normalized electrical field intensity distribution on the entire anodic workpiece surface for SLEMM and TMEMM is showed in Fig.5. It can clearly be concluded that the electrical field intensity distribution within ±2 mm is basically same along the *x* direction on the workpiece surface, and the electrical field intensity distribution increases gradually along the *x* direction of 3~5 mm (-3~-5 mm) on the workpiece surface during TMEMM.

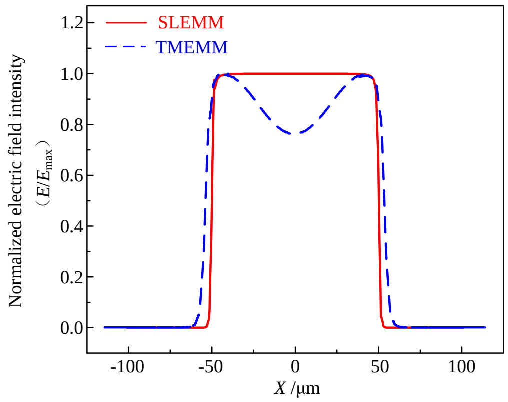

Figure 4. The normalized electrical field intensity distribution within a single through-hole on the initial anodic workpiece surface for SLEMM and TMEMM

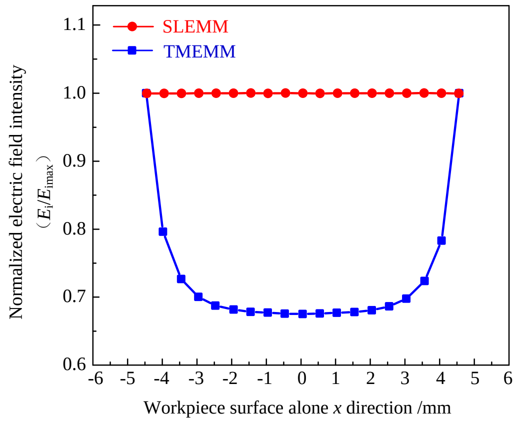

Figure 5. The normalized electrical field intensity distribution on the whole anode workpiece surface for SLEMM and TMEMM

Therefore, the closer to the edge of the anode workpiece, the higher current density, and the faster material removal rate will be, which means that the dimensions of micro-dimples at the edge of the anode workpiece are larger than that at the center of the anode workpiece in TMEMM. However, the electrical field intensity distribution on the anode workpiece surface is uniform, the material removal rate is consistent, and the dimensions of micro-dimples are uniform during SLEMM. Hence, compared with the poor dimensional uniformity of micro-dimples due to the electric field effect in TMEMM, the dimensional uniformity of micro-dimples could be improved because of the even electrical field intensity distribution on the workpiece surface during SLEMM.

2.3 Experimental Investigation

In this investigation, a negative photoresist film of GPM220 dry-film (DuPont, USA) was employed. The photolithography process of the dry-film mask has been reported in detail in previous investigations [21]. The detailed experimental parameters are shown in Table 3. Micro-dimples were machined with a sodium nitrate electrolyte at a concentration of 100 g/L at 25 °C, and the electrolyte conductivity is 8.7 S/m. The current data was acquired with a closed-loop Hall current sensor (CSM050NPT5, Chahua, China) and a data acquisition card (NI PCI-6221, USA). The profile of micro-dimple was measured using a three-dimensional profiler (DVM5000, Leica, Germany) and a scanning electron microscope (SEM) (S-3400N, Hitachi, Japan).

Table 3. The experimental parameters in experimental investigations

Parameter	Value
Diameter of through-holes in dry-film mask	100 μm
Thickness of dry-film mask	50 μm
Electrolyte concentration	100 g/L $NaNO_3$
Electrolyte temperature	25 °C
Electrolyte conductivity	8.7 S/m
Workpiece material	Stainless steel 304
Inter-electrode gap (TMEMM)	2 mm

3. RESULTS AND DISCUSSION

It can be known from our previous investigations that the maximum depth of 4 μm for micro-dimples could be prepared with the increase of applied voltage and machining time, because of the electrolytic products accumulated on the workpiece surface during single-cycle SLEMM. In addition, the machining current decreased sharply within 10 s machining time, due to a large number of nonconductive insoluble electrolytic products accumulated in the enclosed unit of SLEMM [21]. Thus, 10 s machining time is employed as one cycle of SLEMM. Namely, the power supply is turn off and the cathodic tool moves up after 10 s machining time, then the electrolytic products are removed, the electrolyte is renewed in the inter-electrode gap, and the cathodic tool moves down to continue the next cycle machining process of SLEMM.

3.1 Influence of multiple cycles of SLEMM on micro-dimples dimensions

To investigate the influence of multiple cycles of SLEMM on the dimensions of micro-dimples, 30 random data points were measured with micro-dimples machined at the same 15 V applied voltage. Table 4 exhibits the change of dimensions of micro-dimples generated with 1~6 cycles machining process of SLEMM. It can be seen that the mean diameters and depths of micro-dimples increased with multiple SLEMM increased from single-cycle to sixth cycle, in which the mean diameter increased from 103.2 μm to 114.7 μm, and the mean depth varied from 2.93 μm to 12.89 μm.

Table 4. Effect of multiple cycles of SLEMM on micro-dimples dimensions

Machining cycles	Mean depth *h* (μm)	Mean diameter *d* (μm)
1	2.93	103.22
2	5.08	106.86
3	7.64	108.82
4	10.83	110.93
5	12.47	112.04
6	12.89	114.71

The current signal measured with a closed-loop Hall current sensor is shown in Fig. 6. It can be indicated that the initial current decreased with 1~6 cycles machining process of SLEMM, in which the initial current decreased from 1.03 A to 0.61 A. This is because the electrolytic products were removed with high pressure of electrolyte flushed to the workpiece surface, which is conductive to continuous dissolution of workpiece for the next cycle of SLEMM, and then the dimensions in depth direction increased. Therefore, due to the inter-electrode gap increased gradually, the initial current decreased with the increase of machining cycles of SLEMM. In addition, owing to the stray current increased with the prolonging of machining time, and a small amount of electrolytes penetrate into the edge area of the dry-film mask when electrolyte washed the electrolytic products, the overcutting in the diameter direction of micro-dimples increased.

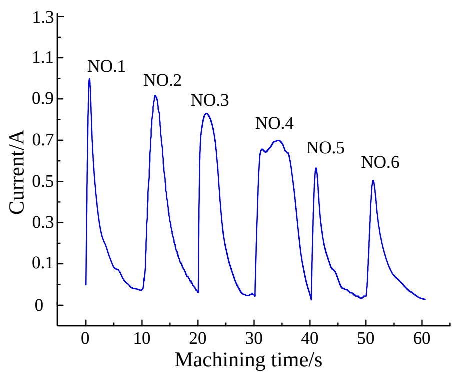

Figure 6. The current signal with 6th cycles process of SLEMM

During each cycle machining process of SLEMM, not only the gas bubbles and nonconductive insoluble electrolytic products produced, but also the electrolytic heat produced. Thus, the integrity of the dry-film mask would be damaged by the combined effects of electrolytic products, electrolytic heat and the pressure of the cathodic tool on the dry-film mask, which means that the dry-film mask could not be reused all the time. The experimental investigations showed that the 12th cycles machining process of SLEMM could be done at the 15 V applied voltage, and the variation of micro-dimples dimensions is listed in Fig. 7. The SEM images and 3D profiles of micro-dimples fabricated with 15 V applied voltage and the 12th process of SLEMM, as shown in Fig. 8, in which the depth and diameter are 18 μm and 120 μm, respectively. Therefore, the deep depth of micro-dimples could be machined with multiple cycles process of SLEMM, compared with single-cycle SLEMM.

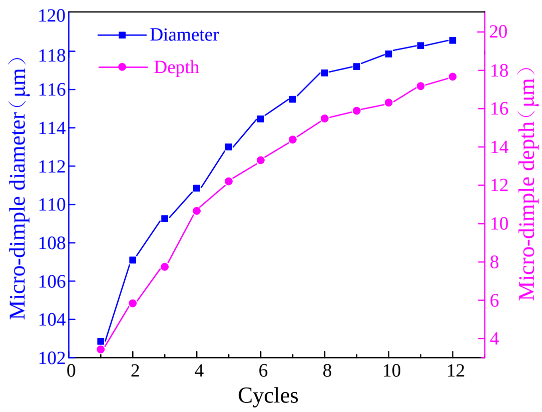

Figure 7. The dimensions of micro-dimples machined with multiple cycles of SLEMM

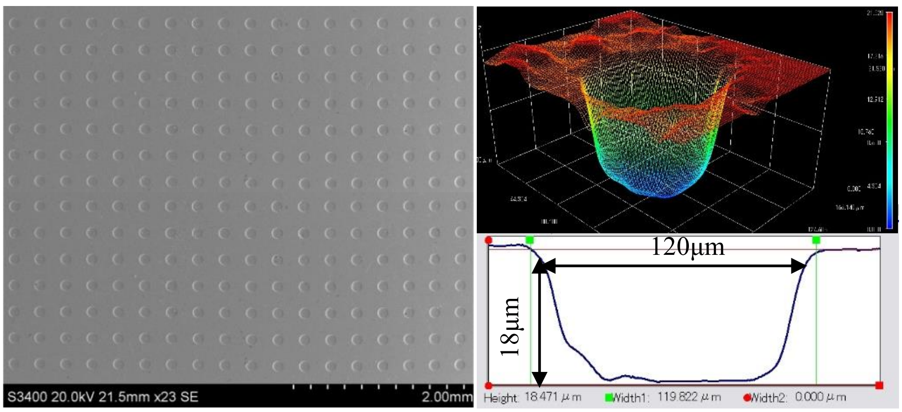

Figure 8. SEM images and 3D profiles of micro-dimple prepared by 12th cycles of SLEMM at the applied voltage of 15 V

3.2 Influence of applied voltage on micro-dimples dimensions

To research the influence of applied voltage on dimensions of micro-dimples, 30 random data points were measured with micro-dimples machined at the same 6th cycles process of SLEMM with the applied voltage in the range of 6~18 V. The variation of micro-dimples dimensions with the increase of applied voltage is listed in Table 5. It can be concluded that the mean diameters and mean depths of micro-dimples increased with the applied voltage increased from 6 V to 18 V, in which the mean diameters varied in the range of 106.9~116.3 μm, and the mean depths varied in the range of 6.36~13.02 μm. This can be attributed to the current density increased with the increase of applied voltage, which means that the material removal rate increased with the increase of applied voltage. The SEM images and 3D profiles of micro-dimples fabricated with 12 V applied voltage and the 6th process of SLEMM, as shown in Fig. 9, in which the depth and diameter are 10 μm and 116 μm, respectively. Therefore, the dimensions of micro-dimples increased with the increase of applied voltage, and deep depth of micro-dimples could be machined during multiple cycles process of SLEMM, compared with the maximum depth of 4 μm for micro-dimples obtained in single-cycle SLEMM.

Table 5. Effect of applied voltage on micro-dimples dimensions at the 6th cycles process of SLEMM

Applied voltage U (V)	Mean depth h (μm)	Mean diameter d (μm)
6	6.36	106.98
9	9.53	110.53
12	10.62	113.68
15	12.89	115.21
18	13.02	116.36

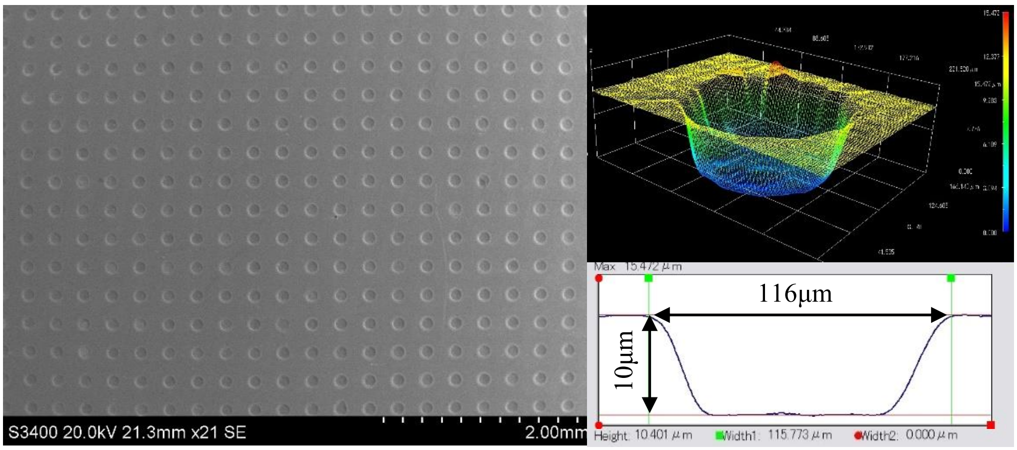

Figure 9. SEM images and 3D profiles of micro-dimple prepared by 6th cycles of SLEMM at the applied voltage of 12 V

3.3 Profiles of micro-dimples machined between TMEMM and SLEMM

To investigate the appearance of micro-dimples, micro-dimple arrays were prepared by TMEMM and SLEMM with the same applied voltage of 15 V. Fig. 10 exhibits the SEM images and 3D profiles of micro-dimple arrays machined with TMEMM and SLEMM. It can clearly be seen that an island formed in the center of the micro-dimples prepared by using TMEMM (see Fig. 10a). The results imply that the current density distribution on the workpiece surface is uneven, and the removal rate at the edge is faster than that at the center, which agrees well with the simulation results in TMEMM. However, for the same micro-dimple depth, micro-dimple arrays with flat bottom were machined by using SLEMM (see Fig. 10b). This is due to the even current density distribution on the workpiece surface during SLEMM. Thus, the experiments prove that the method of SLEMM could avoid the island phenomenon of micro-dimples.

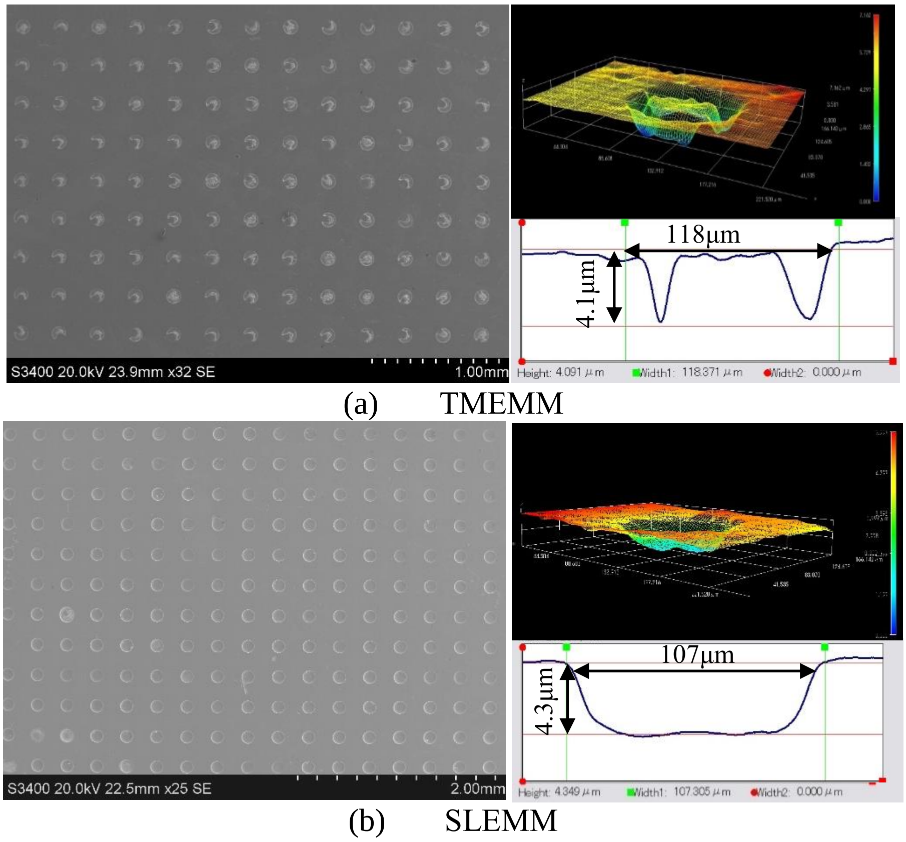

Figure 10. SEM images and 3D profiles of micro-dimple prepared by TMEMM and SLEMM

Moreover, micro-dimples generated using SLEMM have smaller diameters than those fabricated in TMEMM with the same depth of 4 μm, in which the diameter of micro-dimples is 118 μm in TMEMM, and the diameter of micro-dimples is 107 μm during SLEMM. This is because the edge effect of electric field increased the overcutting in the diameter direction of micro-dimples in TMEMM. However, the more uniform electrical field intensity distribution in SLEMM is useful for reducing overcutting in the micro-dimple diameter, compared with TMEMM. In addition, the nonconductive insoluble electrolytic products and gas bubbles accumulated on the workpiece surface in the enclosed unit inhibited the dissolution of in the diameter direction during SLEMM [21]. Therefore, the method of SLEMM could not only remove island defect of micro-dimples generated in TMEMM, but also improve the machining accuracy of micro-dimples

The SEM images and the dimensions of micro-dimples from the center to the edge are shown in Fig. 11, in which the micro-dimples machined using TMEMM with 16 V applied voltage at an inter-electrode gap of 2 mm, and the micro-dimples generated with 4th cycles process of SLEMM at 16 V applied voltage. It can be concluded that the dimensions of micro-dimples at the edge is higher than that in other areas in TMEMM. The micro-dimple diameter and depth are 121 and 11 μm, respectively, at the center of the workpiece surface. However, they become 131 and 16 μm, respectively, at the edge. However, the diameter and depth of micro-dimples at the center are almost the same as those of the micro-dimples at the edge, with values of 110 μm in diameter and 11 μm in depth, respectively. This is because the electrical field intensity at the edge is higher than that in other areas on the workpiece surface, which results in non-uniform dimensional distribution of micro-dimples during TMEMM. However, the even electrical field intensity distribution is beneficial in improving dimensional uniformity of micro-dimples in SLEMM, compared with TMEMM.

A 250 μm thick PDMS mask has been applied to enhance the electrical field intensity distribution on the anode workpiece surface and to remove the island of micro-dimples fabricated in TMEMM [24]. In addition, the escape of oxygen bubbles accumulating at the edges of micro-dimples inhibited continuous dissolution in radial direction, greatly reducing undercutting in TMEMM with the thick PDMS mask [25]. However, utilizing the thick PDMS mask involves a considerable amount of expense, and PDMS mask being hydrophobic in nature may restrict the electrolyte flow into the through-holes on the mask. The method of multiple SLEMM is convenient to improve the machining accuracy of micro-dimples.

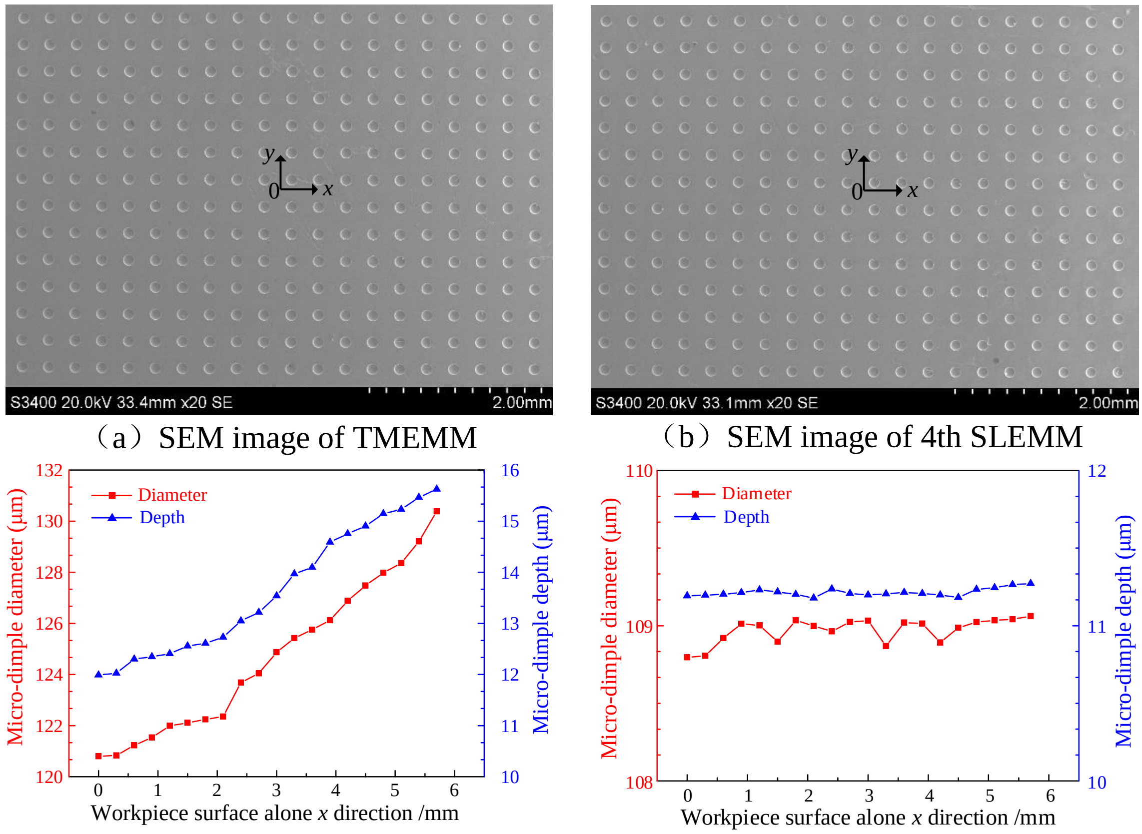

(a) SEM image of TMEMM (b) SEM image of 4th SLEMM

(c) Dimensions of micro-dimples in TMEMM (d) Dimensions of micro-dimples of 4th SLEMM

Figure 11. SEM images and 3D profiles of micro-dimple prepared by TMEMM and 4th cycles of SLEMM

4. CONCLUSIONS

The multiple cycles process of SLEMM has been explored to generate micro-dimples. According to the numerical simulations and experimental investigations, the conclusions can be summarized as follows:

1. The numerical simulation results demonstrate that a mutational electrical field intensity

distribution occurs at the mask edge and that the distribution is more uniform on the anode workpiece surface in SLEMM, compared with TMEMM.

2. Compared with the maximum depth of 4 μm for micro-dimples generated with the increase of machining time, applied voltage in single-cycle of SLEMM, the dimensions of micro-dimples increased with the increase of applied voltage, and deep depth of micro-dimples could be machined during multiple cycles process of SLEMM. And at 15 V applied voltage and the 12th cycles process of SLEMM, the depth and diameter are 18 μm and 120 μm, respectively.

3. Due to the more even electrical field intensity distribution in SLEMM, the experimental results show that the method of SLEMM could not only remove island defect of micro-dimples generated in TMEMM, but also improve dimensional uniformity of micro-dimples.

ACKNOWLEDGMENTS
The work described in this study was supported by the Foundation for Young Scholars of Jiangsu Province, China (Grant BK20180969), the Natural Science Foundation of the Jiangsu Higher Education Institution of China (Grant 18KJB460025), and the Suzhou Science and Technology project (Grant SYG201644).

References

1. A. Ronen, I. Etsion, Y. Kligerman, *Tribology Transactions*, 44 (2001) 359-366
2. M. Cho, *Wear*, 346 (2016) 158-167
3. D.W. Wang，J.L. Mo，Z.G. Wang, *Journal of Mechanical Engineering*, 49 (2013) 112-116
4. Q.W. Dai，W. Huang, X.L. Wang, *Experimental Thermal and Fluid Science*, 57 (2014) 200-206
5. H.P. Syahputra, T.J. Ko, *Journal of Precision Engineering and Manufacturing*, 14 (2013) 1507-1512
6. R. Kurniawan, T.J. Ko, *International Journal of Precision Engineering and Manufacturing*, 14 (2013)199-206
7. J.Y. Zhang, Y.G. Meng, *Journal of Materials Processing Technology*, 212 (2012) 2133-2140
8. A. Cunha, A.M. Elie, L. Plawinski, *Applied Surface Science*, 360 (2016) 485-493
9. L.M. Vilhena, A. Ramalho, A. Cavaleiro, *Lubrication Science*, 29 (2017) 493-501
10. C. Winkelmann, W. Lang, *International Journal of Machine Tools and Manufacture*, 72 (2013) 25-31
11. C. Madore, D. Landolt, *Journal of Micromechanics and Microengineering*, 7 (1997) 270
12. X.Q. Hao, L. Wang, Q.D. Wang, *Applied Surface Science*, 257 (2011) 8906–8911
13. S. Nouraeiz, S. Roy, *Journal of The Electrochemical Society*, 155 (2008) D97–D103
14. J.G. Parreira, C.A. Gallo, H.L. Costa, *Surface and Coatings Technology*, 212 (2012) 1–13
15. D. Zhu, N.S. Qu, H.S. Li, Y.B. Zeng, D.L. Li, S.Q. Qian, *CIRP Annals-Manufacturing Technology*, 58 (2009) 177–180
16. X.L. Chen, N.S. Qu, H.S. Li, Z.Y. Xu, *Journal of Materials Processing Technology*, 229 (2016) 102–110
17. T. Roy, D. Choudhury, A.B. Mamat, *Ceramics International*, 40 (2014)2381–2388
18. R.V. Shenoy, M. Datta, *Journal of the Electrochemical Society*, 143 (1996) 544-549
19. L. Wang, Q.D. Wang, X.Q. Hao, *The International Journal of Advanced Manufacturing Technology*, 51 (2010) 155-162
20. X.L. Chen, N.S. Qu, H.S. Li, *The International Journal of Advanced Manufacturing Technology*, 80 (2015) 1577-1585

21. X.F. Zhang, N.S. Qu, X.L. Fang, *Surface and Coatings Technology*, 311 (2017) 357-364
22. X. Feng, J.Z. Zhou, Y.F. Mei, *Chinese Journal of Mechanical Engineering*, 28 (2015) 904-910
23. J. Li, S. Liu, A. Yu, *Tribology International,* 118 (2018) 37-45
24. X.L. Chen, N.S. Qu, H.S. Li, Z.N. Guo, *Precision Engineering*, (39) 2015 204-211
25. X.L. Chen, N.S. Qu, X.L. Fang, D. Zhu, *Surface and Coatings Technology*, 277 (2015) 44-51